Long-term model predictive control of gene expression at the population and single-cell levels

Jannis Uhlendorf, Agnès Miermont, Thierry Delaveau, Gilles Charvin, Francois Fages, Samuel Bottani, Grégory Batt, Pascal Hersen

Long-term model predictive control of gene expression at the population and single-cell levels

Jannis Uhlendorf[a,b], Agnès Miermont[b], Thierry Delaveau[c], Gilles Charvin[d], François Fages[a], Samuel Bottani[b], Gregory Batt[a,1,2], and Pascal Hersen[b,e,1,2]

[a]Contraintes Research Group, Institut National de Recherche en Informatique et en Automatique, INRIA Paris-Rocquencourt, 78150 Rocquencourt, France; [b]Laboratoire Matière et Systèmes Complexes, Unité Mixte de Recherche 7057 Centre National de la Recherche Scientifique and Université Paris Diderot, 75013 Paris, France; [c]Laboratoire de Génomique des Microorganismes, Unité Mixte de Recherche 7238 Centre National de la Recherche Scientifique and Université Pierre et Marie Curie, 75006 Paris, France; [d]Institut de Génétique et Biologie Moléculaire et Cellulaire, 67400 Illkirch, France; and [e]Mechanobiology Institute, National University of Singapore, Singapore 117411

Edited by David A. Weitz, Harvard University, Cambridge, MA, and approved July 16, 2012 (received for review April 23, 2012)

Gene expression plays a central role in the orchestration of cellular processes. The use of inducible promoters to change the expression level of a gene from its physiological level has significantly contributed to the understanding of the functioning of regulatory networks. However, from a quantitative point of view, their use is limited to short-term, population-scale studies to average out cell-to-cell variability and gene expression noise and limit the nonpredictable effects of internal feedback loops that may antagonize the inducer action. Here, we show that, by implementing an external feedback loop, one can tightly control the expression of a gene over many cell generations with quantitative accuracy. To reach this goal, we developed a platform for real-time, closed-loop control of gene expression in yeast that integrates microscopy for monitoring gene expression at the cell level, microfluidics to manipulate the cells' environment, and original software for automated imaging, quantification, and model predictive control. By using an endogenous osmostress responsive promoter and playing with the osmolarity of the cells environment, we show that long-term control can, indeed, be achieved for both time-constant and time-varying target profiles at the population and even the single-cell levels. Importantly, we provide evidence that real-time control can dynamically limit the effects of gene expression stochasticity. We anticipate that our method will be useful to quantitatively probe the dynamic properties of cellular processes and drive complex, synthetically engineered networks.

model based control | computational biology | high osmolarity glycerol pathway | quantitative systems biology

Understanding the information processing abilities of biological systems is a central problem for systems and synthetic biology (1–6). The properties of a living system are often inferred from the observation of its response to static perturbations. Time-varying perturbations have the potential to be much more informative regarding the dynamics of cellular functions (7–12). Currently, it is not possible to precisely perturb protein levels in an analogous manner, even though this perturbation would be instrumental in our understanding of gene regulatory networks. Indeed, despite the development of novel regulatory systems, including various RNA-based solutions (13), transcriptional control by means of inducible promoters is still the preferred method for manipulating protein levels (14, 15). Unfortunately, inducible promoters have several generic limitations. First, there is a significant delay between gene expression activation and effective protein synthesis. Second, many cellular processes can interfere with gene expression through internal feedback loops whose effects are hard to predict. Third, the process of gene expression shows significant levels of noise (16–18). Given these limitations, novel experimental strategies are required to gain quantitative, real-time control of gene expression in vivo.

Here, we see the problem of manipulating gene expression to obtain given temporal profiles of protein levels as a model-based control problem. More precisely, we investigate the effectiveness of computerized closed-loop control strategies to control gene expression in vivo. In model-based closed-loop control, a model of the system is used to constantly update the control strategy based on real-time observations. We propose an experimental platform that implements such an in silico closed loop in the budding yeast *Saccharomyces cerevisiae*. We show that gene expression can be controlled by repeatedly stimulating a native endogenous promoter over many cell generations (>15 h) for both time-constant and time-varying target profiles and at both the population and single-cell levels. Recently, Milias-Argeitis et al. (19) also proposed an approach for feedback control of gene expression in yeast. In contrast to their work, we propose a method that is effective at the single-cell level, for time-varying target profiles, and robust despite the presence of strong internal feedback loops. We start by describing the gene induction system and the experimental platform before discussing its efficiency.

Results and Discussion

Controlled System. We based our approach on the well-known response of yeast to an osmotic shock, which is mediated by the high osmolarity glycerol (HOG) signaling cascade. Its activation leads to the phosphorylation of the protein Hog1 (Fig. 1*A*), which orchestrates cell adaptation through glycerol accumulation. Phosphorylated Hog1 promotes glycerol production by activating gene expression in the nucleus as well as stimulating glycerol-producing enzymes in the cytoplasm. After they are adapted, the cells do not sense the hyperosmotic environment anymore, the HOG cascade is turned off, and the transcriptional response stops (20–22). In control terms, yeast cells implement several short-term (non transcriptional) and long-term (transcriptional) negative feedback loops that ensure perfect adaptation to the osmotic stress (10, 23). Because of these adaptation mechanisms, it is a priori challenging to control gene expression induced by osmotic stress. It is, thus, an excellent system to show that one can robustly control protein levels, even in the presence of internal negative feedback loops. Several genes are up-regulated in response to a hyperosmotic stress. These genes include the nonessential gene *STL1*, which codes for a glycerol proton symporter (24, 25). We decided to use its native promoter (pSTL1) to drive the expression of yECitrine, a fluorescent reporter. Applying an osmotic stress transiently activated the HOG cascade (Fig. 1*B*), and yECitrine levels reached modest values (600 fluorescence units) (Fig. 1*B*). Importantly, when short but repeated stresses were applied, pSTL1 could be repeatedly activated, and much higher levels could be reached (Fig. 1*C*).

Author contributions: J.U., G.B., and P.H. designed research; J.U. performed research; J.U., A.M., T.D., G.C., F.F., S.B., G.B., and P.H. contributed new reagents/analytic tools/software; J.U., G.B., and P.H. analyzed data; and J.U., G.B., and P.H. wrote the paper.

The authors declare no conflict of interest.

This article is a PNAS Direct Submission.

Freely available online through the PNAS open access option.

[1]To whom correspondence may be addressed. E-mail: gregory.batt@inria.fr or pascal.hersen@univ-paris-diderot.fr.

[2]G.B. and P.H. contributed equally to this work.

This article contains supporting information online at www.pnas.org/lookup/suppl/doi:10.1073/pnas.1206810109/-/DCSupplemental.

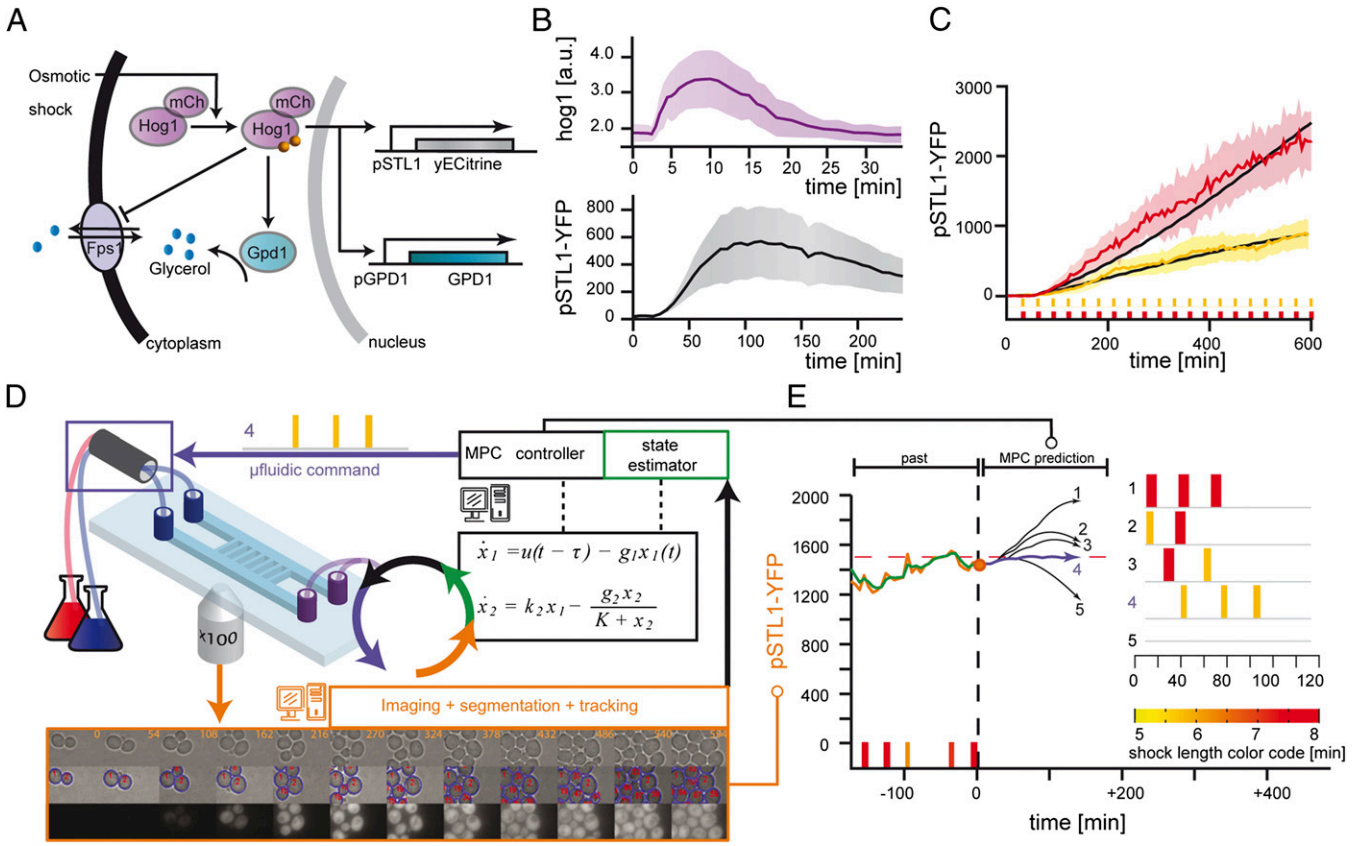

Fig. 1. A platform for real-time control of gene expression in yeast. (*A*) A hyperosmotic stress triggers the activation and nuclear translocation of Hog1. Short-term adaptation is mainly implemented by cytoplasmic activation of the glycerol-producing enzyme Gpd1 and closure of the aqua-glyceroporin channel Fps1. Long-term adaptation occurs primarily through the production of Gpd1. (*B*) When maintained in a hyperosmotic environment (1 M sorbitol), the HOG cascade was quickly activated, which is seen by Hog1 nuclear enrichment. This transient signaling response lasted typically <20 min. The expression level of pSTL1-yECitrine (YFP) increased after an ~20-min delay, peaked around 600 fluorescence units after 100 min, and then decayed. (*C*) In contrast, the fluorescence level showed a continuous increase when stimulated periodically (T = 30 min). The increase rate was larger for longer pulses (red, 8 min; yellow, 5 min). Black curves are the expected behaviors based on our model of the pSTL1 induction. Solid lines and their envelopes are the experimental means and SDs of the cells' fluorescence. (*D*) Yeast cells grew as a monolayer in a microfluidic device that was used to rapidly change the cells' osmotic environment (blue frame) and image their response. Segmentation and cell tracking were done using a Hough transform (orange frame). The measured yECitrine fluorescence, either of a single cell or of the mean of all cells, was then sent to a state estimator connected to an MPC controller. A model (black frame) of pSTL1 induction was used to find the best possible series of osmotic pulses to apply in the future so that the predicted yECitrine level follows a target profile. (*E*) At the present time point (orange circle), the system state is estimated (green), and the MPC searches for the best input (pulse duration and number of pulses) (see text and *SI Materials and Methods*), which minimizes the distance of the MPC predictions (black curves) to the target profile (red dashed line) for the next 2 h. Here, the osmotic series of pulses that corresponds to the blue curve (4) was selected and sent to the microfluidic command. This control loop is iterated every 6 min.

A closed-loop control of the pSTL1 activity requires the acquisition and analysis of live cell images, the computation of the input (i.e., osmolarity) to be applied in the near future, and the ability to change the cells osmotic environment accordingly (Fig. 1 *D* and *E*).

Experimental Platform. To observe the cells and control their environment, we designed a versatile platform made of standard microscopy and microfluidic parts. The microfluidic device contained several 3.1-μm-high chambers that were connected by both ends to large channels through which liquid media could be perfused (Fig. 1*D*). Because the typical diameter of an *S. cerevisiae* cell is 4–5 μm, the cells were trapped in the chamber and grew as a monolayer. Their motion was limited to slow lateral displacement due to cell growth (Fig. S1). This design allowed for long-term cell tracking (>15 h) and relatively rapid media exchanges (~2 min). The HOG pathway was activated by switching between normal and sorbitol-enriched (1 M) media.

Model of pSTL1 Induction. To decide what osmotic stress to apply at a given time, we used an elementary model of pSTL1 induction. Many models have been proposed for the hyperosmotic stress response in yeast (10, 26–30). We used a generic model of gene expression written as a two-variable delay differential equation system, where the first variable denotes the recent osmotic stress felt by the cell and the second variable is the protein fluorescence level (Fig. 1*D*, *Materials and Methods*, Table S1, and *SI Materials and Methods*). Because our goal was to show robust control, despite the presence of unmodeled feedback loops, the adaptation mechanisms described above were purposefully neglected. The choice of this model was also motivated by the tradeoff between its ability to quantitatively predict the system's behavior (favors complexity) and the ease of solving state estimation problems (favors simplicity). Despite its simplicity, we found a fair agreement between model predictions and calibration data corresponding to fluorescence profiles obtained by applying either isolated or repeated osmotic shocks of various durations (Fig. 1*C* and Fig. S2).

Closing the Loop. The fluorescence intensity of a single cell arbitrarily chosen at the start of the experiment, or the average fluorescence intensity of the cell population, was sent to a state estimator (extended Kalman filter discussed in *SI Materials and Methods*) connected to a model predictive controller (31). Model Predictive Control (MPC) is an efficient framework well-adapted

to constrained control problems. Schematically, given a model of the system and desired temporal profiles for the system's outputs, MPC aims at finding inputs to minimize the deviation between the outputs of the model and the desired outputs. The control strategy is applied for a (short) period. Then, the new state of the system is observed, and this information is used to compute the control strategy to be applied during the next time interval. This receding horizon strategy yields an effective feedback control. In practice, every 6 min, given the current estimate of the system state, past osmotic shocks, and our model of gene expression, the controller searched for the optimal number of osmotic pulses to apply within the next 2 h and their optimal start times and durations (Fig. 1*E*). If a shock had to be applied within the next 6 min, then it was applied. Otherwise, the same computation was reiterated 6 min later based on new observations, thus effectively closing the feedback loop. Here, we dealt with short-term cell adaptation by imposing a maximal stress duration of 8 min and a 20-min relaxation period between consecutive shocks. Under such conditions, cells stay responsive to osmotic stress at all times (Fig. 1*C*). This can be explained by the fact that, in absence of stress, the glycerol channel Fps1 opens (21, 32) and lets the glycerol leak out of the cell, thus effectively resetting the osmotic state of the cells (29).

Note that a proportional integral (PI) controller would have been an attractive alternative, because it would not have required the development of a model of the system. With PI controllers, the applied input (i.e., stress) is simply the weighted sum of the current error (deviation between target and measured outputs) and the integral of the (recent) past errors. Consequently, using a PI controller to reach high levels of fluorescence would lead to a control strategy in which high stress is maintained over extended periods of time. This condition would trigger cell adaptation and eventually lead to a stalled situation in which the maximal stress is applied without any effect.

Closed-Loop Population Control Experiments. Our first goals were to maintain the average fluorescence level of a cell population at a given constant value (set-point experiment) and force it to follow a time-varying profile (tracking experiment). Both types of experiments lasted at least 15 h, starting with a few cells and ending with 100–300 cells in the field of view (Fig. S3). The control objective was to minimize the mean square deviations (MSDs) between the mean fluorescence of the population of cells and the target profile. We succeeded in maintaining the average fluorescence level at a given constant value or forcing it to follow several given time-varying profiles (Fig. 2 *A*–*D*, Figs. S3, S4, and S5, and Movies S1, S2, and S3). Admissible time-varying target profiles were obviously constrained by the intrinsic timescales of the system, such as the maximal protein production and degradation rates. However, within these constraints, graded responses could be obtained. In Fig. 2*C*, for example, the trapeze slope is less steep than what maximal pSTL1 induction can deliver (Fig. 2 *A* and *B*). Note that our control strategy opened the possibility to reach higher fluorescence levels than what full induction with a step shock would allow (compare with Fig. 1*B*). Indeed, because of cell perfect adaptation to hyperosmotic stresses, a sustained 1 M sorbitol shock triggers only a transient gene expression and fluorescence peaks at moderate levels (Fig. 1*B*). By using repeated, well-separated pulses,

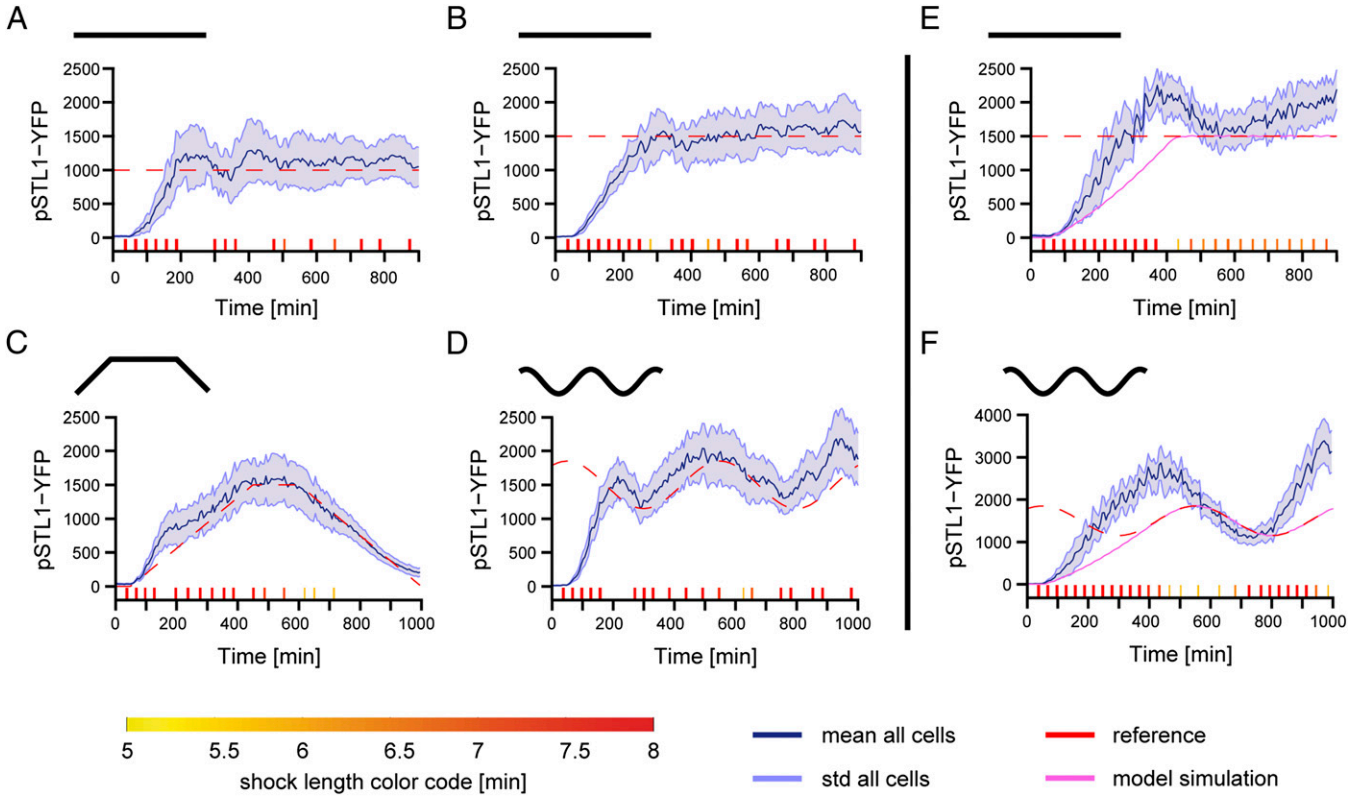

Fig. 2. Real-time control of gene expression can be achieved at the population level. (*A* and *B*) Set-point control experiments with target values 1,000 and 1,500 fluorescence units (f.u.; red dashed line). This unit is the same across all graphs (no renormalization). To avoid desensitizing the HOG pathway, the controller repeatedly applied short osmotic pulses (durations between 5 and 8 min). The timeline of osmotic events is shown at the bottom of each graph (color code along the bottom). Shock starting times and durations were computed in real time. The measured mean cell fluorescence is shown as solid blue lines. The envelopes indicate SD of the fluorescence distribution across the yeast population. (*C* and *D*) Tracking control experiments. In *C*, the target has a trapezoidal shape (maximum at 1,500 f.u.). In *D*, the target is sinusoidal (average value at 1,500 f.u.). In both cases, the mean level of fluorescence successfully follows the time-varying target profile. (*E* and *F*) Open-loop control experiments. Two examples of open-loop control (the osmotic inputs were computed using our model before starting the experiments) showing poor control quality. Errors accumulate over time. The simulated behavior of the system is represented in violet.

pSTL1 was iteratively activated (Fig. 1*C* and Movie S4). To assess the effective control range, we performed additional control experiments with target values spanning an order of magnitude (200–2,000 fluorescence units) (Fig. S5). Despite an initial overshoot for the lower target (200 fluorescence units), our results showed good control accuracy over time.

Quantitative limitations of our experimental platform can originate from the model, the state estimator, the control algorithm, and the intrinsic biological variability of gene expression. In silico analysis showed that applying the proposed control strategy to the (estimated state of the) system resulted in control performances that were significantly better than those obtained experimentally (Fig. 2 *E* and *F* and Fig. S4). Therefore, the control algorithm performed well, and future improvements should focus on system modeling and state estimation to better represent the experimental state of the system. To assess the importance of biological variability and modeling limitations, we carried out open-loop control experiments with the same objectives and the same model of the system. A time series of osmotic pulses was computed before the experiment and then sent to yeast cells without performing real-time corrections. Important deviations were found, indicating clear discrepancies between model predictions and the long-term system behavior (Fig. 2 *E* and *F*). As expected, open-loop strategies cannot result in a quantitative, robust control of gene expression. In contrast, closed-loop control performs well, despite significant biological variability and/or limited model accuracy.

Closed-Loop Single-Cell Control Experiments. In a second set of experiments, we focused on the real-time control of gene expression at the single-cell level. We tracked one single cell over at least 15 h and used its fluorescence to feed the MPC controller. As shown in Fig. 3, we obtained results with quality that is out of reach of any conventional gene induction system, both for constant and time-varying target profiles (Movies S5, S6, and S7). Because of intrinsic noise in gene expression, single-cell control was a priori more challenging than population control. Indeed, compared with the mean fluorescence levels in population control experiments, the fluorescence levels of controlled cells in single-cell control experiments showed larger fluctuations around the target values. However, at the cell level, the MSDs of controlled cells obtained in single-cell control experiments were significantly smaller than the MSDs of a cell in population control experiments (Fig. 4*B*, *SI Materials and Methods*, Table S2, and Fig. S6). For set-point control experiments in which fluctuations happen around a fixed reference value, we also defined the fluorescence noise level as the standard deviation (SD) over the mean. Again, we found that single-cell control significantly decreased noise at the cell level (Fig. 4*C*, *SI Materials and Methods*, Table S2, and Fig. S6). Taken together, these results show that real-time control effectively improves control quality and counteracts the effects of noise in gene expression when performed at the single-cell level. Interestingly, single-cell control experiments showed that, in few cases, the controlled cell behaved significantly differently from the rest of the population over extended periods of time (e.g., see Fig. 3*A*), suggesting long-term memory effects for gene expression spanning many cell generations. Lastly, the fact that, for different controlled cells but the same control objective, the decisions of the closed-loop controller were markedly different (Fig. 3*E*) highlights the fact that feedback control was critical to achieve good control performance at the single-cell level. This suggests that cell-to-cell variability and noise in gene expression fundamentally limit the quality of any open-loop inducible system.

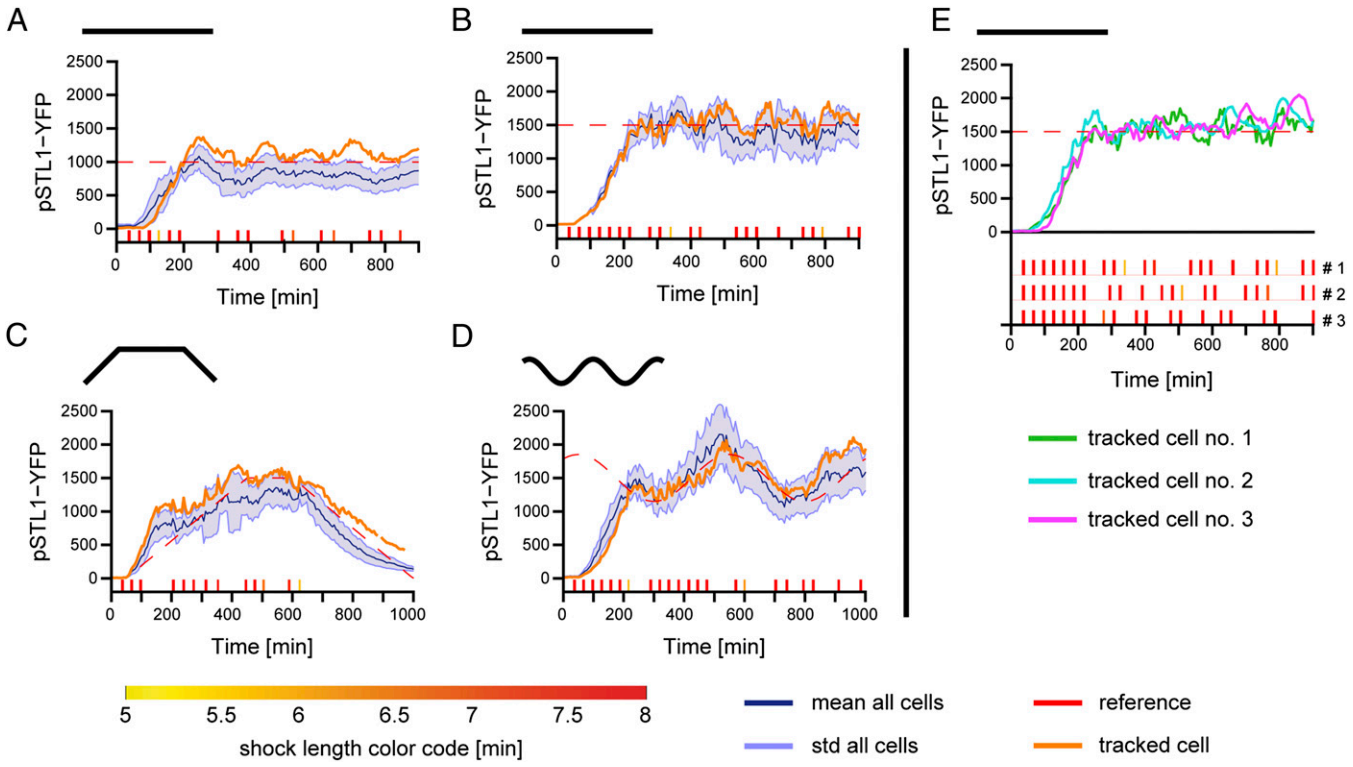

Fig. 3. Real-time control of gene expression can be achieved at the single-cell level. (*A* and *B*) Set-point control experiments at values 1,000 and 1,500 f.u. The yECitrine fluorescence of the controlled cells is shown as orange lines. The blue line and its envelope indicate the mean fluorescence and the SD of the fluorescence across the cell population. The population follows the target profile but with less accuracy than the controlled single cell. (*C* and *D*) Tracking control experiments. In *C*, the target has a trapezoidal shape (maximum at 1,500 f.u.). In *D*, the target is sinusoidal (average at 1,500 f.u.). (*E*) The fluorescence of the controlled cell in three different single-cell control experiments is represented together with the osmolarity profiles that were applied. Different experiments are labeled with different colors, and therefore, their corresponding osmotic inputs can be identified. It appears that, for each cell, the controller decisions were markedly different, showing that cell-to-cell variability was at play and that feedback control was critical when performing single-cell control.

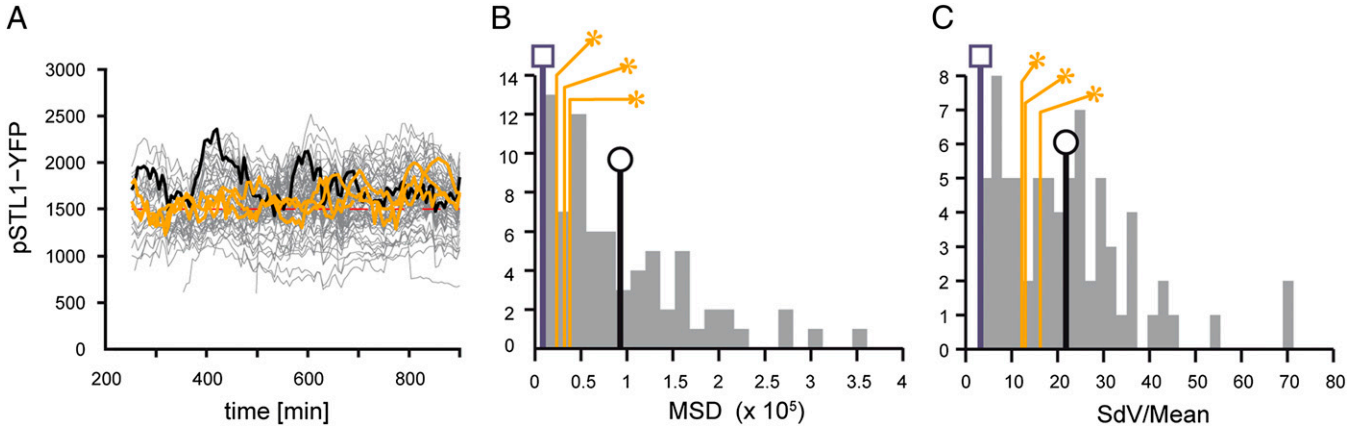

Fig. 4. Effectiveness of closed-loop control. (*A*) Single-cell fluorescence time profiles in two population control experiments (thin gray lines) and three single-cell control experiments (thick orange lines). One representative trace of a single cell in a population control experiment is shown in black. (*B*) Distribution of the MSDs of individual cells in population control experiments (gray). MSDs are defined with respect to the target profiles. The orange bars (stars) show the MSDs for the controlled cells in three single-cell control experiments. These data are compared with the mean MSD of single cells when controlling the population (black line, circle), which shows lower control quality. As expected, the control quality of the population is better (blue line, square), because noise in gene expression is averaged out. (*C*) Distribution of the noise levels defined as the ratio of the SD to the mean. Lower noise levels are observed for controlled cells in single-cell control experiments (orange, star) than a random cell in population control experiments (black line).

Conclusions

We showed that gene expression can be controlled in real time with quantitative accuracy at both the population and single-cell levels by interconnecting conventional microscopy, microfluidics, and computational tools. Importantly, we provided evidence that real-time control can dynamically limit the effects of gene expression stochasticity when applied at the single-cell level. This model predictive control framework overcame the presence of a significant delay between the environmental change and the fluorescent protein observation and the action of strong non-modeled endogenous negative feedback loops. The fact that good control results can be obtained in a closed-loop setting with a relatively coarse model of an endogenous promoter (compare with open-loop results) suggests that extensive modeling will not be required to transpose our approach to other endo- and exogenous induction systems (e.g., the galactose, methionine, or tetracycline inducible promoters). To appreciate the difficulty of the control problems that we addressed, one should keep in mind that the controlled system, a yeast cell, is an extremely complex and partially known dynamical system and that the controlled process, gene expression, is intrinsically stochastic.

Despite the fact that the importance of control theory for systems and synthetic biology has been widely recognized for more than a decade (33, 34), the actual use of in silico feedback loops to control intracellular processes has only been proposed recently. In 2011, we showed that the signaling activity in live yeast cells can be controlled by an in silico feedback loop (35). Using a PI controller, we controlled the output of a signal transduction pathway by modulating the osmotic environment of cells in real time. A similar framework has been proposed by Menolascina et al. (36). More recently, Toettcher et al. (37) used elaborate microscopy techniques and optogenetics to control (in real time and the single-cell level) the localization and activity of a signal transduction protein (PI3K) in eukaryotic cells. Interestingly, they were able to buffer external stimuli and clamp phosphatidylinositol (3,4,5)-triphosphate (PIP3) levels for short time scales. Because these two frameworks necessitate image acquisition at a high frequency, they are not suitable for long-term experiments. The most closely related work is the work by Milias-Argeitis et al. (19). Using optogenetic techniques, Milias-Argeitis et al. (19) managed to control the expression of a yeast gene to a constant target value over a few hours. Their approach is based on a chemostat culture and well-adapted for biotechnological applications, such as the production of biofuels or small-molecules. However, because it does not allow for single-cell tracking and control, it is less adapted to probe biological processes in single-cell quantitative biology applications. Controlling small cell populations, or even single cells, may be needed in multicellular systems, where cells differ by their genotype (38) or physical location (39).

Connecting living cells to computers is a promising field of research both for applied and fundamental research. By maintaining a system around specific operating points or driving it out of its standard operating regions, our approach offers unprecedented opportunities to investigate how gene networks process dynamical information at the cell level. We also anticipate that our platform will be used to complement and help the development of synthetic biology through the creation of hybrid systems resulting from the interconnection of in vivo and in silico computing devices.

Material and Methods

Yeast Strains and Plasmids. All experiments were performed using a pSTL1::yECitrine-HIS5, Hog1::mCherry-hph yeast strain derived from the S288C background. Cells were cultured overnight in synthetic complete (SC) medium at 30 °C; 4 h before loading them into the microfluidic chip, 60 μL overnight culture were diluted into 5 mL SC, thus obtaining an OD of ~0.19. During the experiment, cell growth continued, with a doubling time between 100 and 250 min (*SI Materials and Methods* and Movies S1, S2, S3, S4, S5, S6, and S7).

Microfluidics. We microfabricated a master wafer by standard soft lithography techniques. A microfluidic chip was made by casting polydimethylsiloxane (PDMS) (Sylgard 184 kit; Dow Corning) on the master wafer, curing it at 65 °C overnight, pealing it off, and bonding it to a glass coverslip after plasma activation. Cells were loaded into the imaging chamber by syringe injection. This created a positive pressure, which let the cells enter the trap. Liquid medium was flown by aspiration into the device using a peristaltic pump (IPC-N; Ismatec) placed after the microfluidic device. We used a flow rate of 230 μL/min. A computer-controlled three-way valve (LFA series; The Lee Company) was used to select between regular medium (SC) or the same medium supplemented with 1 M sorbitol. A switch of the valve state did not lead to an instantaneous change of the cells' environment inside the microfluidic device: a certain time (depending on the flow rate) was needed for the fluid to pass from the valve to the channels and the imaging chamber (Fig. S1).

Microscopy and Experimental Setup. We used an automated inverted microscope (IX81; Olympus) equipped with an X-Cite 120PC fluorescent illumination system (EXFO) and a QuantEM 512 SC camera (Roper Scientific). The YFP filters used were HQ500/20× (excitation filter; Chroma), Q515LP (dichroic; Chroma), and HQ535/30M (emission; Chroma). All these components were driven by the open-source software μManager (40), a plug-in of ImageJ (41), which we interfaced with Matlab using in-house–developed code. The temperature of the microscope chamber, which also contained the media reservoirs, was constantly held at a temperature of 30 °C by a temperature control

system (Life Imaging Services). Images were taken with a 100× objective (PlanApo 1.4 NA; Olympus). The fluorescence exposure time was 200 ms, with fluorescence intensity set to 50% of maximal power. The fluorescence exposure time was chosen such that the fluorescent illumination did not cause noticeable effects on cellular growth over extended periods of time. Importantly, illumination, exposure time, and camera gain were not changed between experiments, and no data renormalization was done. Therefore, the fluorescence intensities can be directly compared across experiments.

Image Analysis. The cellular boundaries were identified on the bright-field image using a circular Hough transform implemented in Matlab (42). For tracking, we compared the current image with the previous one, defined a cell-to-cell distance matrix, and used linear optimization to match pairs of cells. The tracking process was made more robust by also considering the last but one image if a gap was detected (caused by rare segmentation errors). The YFP fluorescence level in each cell was defined as the mean fluorescence level taken over the cell area after subtraction of the background fluorescent level. The signaling activity of the Hog1 cascade can be estimated by measuring the Hog1 nuclear enrichment. We defined the nuclear enrichment of Hog1::mCherry as the difference between the minimal and maximal fluorescence intensities within a cell. Maximal and minimal Hog1::mCherry intensities were computed by averaging the fluorescence of the 15 brightest and 15 dimmest pixels, respectively.

Modeling. The controller used a two dimensional ordinary differential equation (ODE) model to predict the behavior of the system:

$$\dot{x}_1 = u(t-\tau) - g_1 x_1$$

and

$$\dot{x}_2 = k_2 x_1 - g_2 \frac{x_2}{K + x_2},$$

where x_1 denotes the recent osmotic stress and x_2 denotes the protein fluorescence level. The osmotic input (u) is shifted by $\tau = 20$ min to account for the observed delay in the system. The remaining parameters have been estimated based on several calibration experiments: $g_1 = 4.02 \times 10^{-3}$, $k_2 = 0.58$, $g_2 = 37.5$, $K = 750$, and $\tau = 20$ (*SI Materials and Methods*, Table S1, and Fig. S2).

State Estimation. We implemented an extended Kalman filter, which estimates the system state based on fluorescent observations and the model of the system. The parameters of the filter (measurement noise R and process noise Q) were set to $R = 2{,}500$ and $Q = \mathrm{diag}(0.37, 925)$.

Model Predictive Control. The controller searches for osmolarity profiles that minimize the squared deviations between model output and target profile within the next 120 min, while fulfilling the input constraints (pulse duration of 5 to 8 min separated by at least 20 min). In practice, this problem is recast into a parameter search problem, in which parameters are used for encoding stress starting times and shock durations and solved using the global optimization tool CMAES. Because image analysis and parameter search may take up to 3 min, the input to be applied is not immediately available at the time of the measurement. Consequently, we apply at time t the input that was computed at time $t - 3$ min.

ACKNOWLEDGMENTS. The authors acknowledge discussions with D. di Bernardo (Tigem), P.-Y. Bourguignon (Max Planck), S. Léon (Institut Jacques Monod & Centre National de la Recherche Scientifique), F. Devaux, M. Garcia (Université Pierre et Marie Curie), J. M. di Meglio, A. Prastowo (Matière et Systèmes Complexes), R. Bourdais (Supélec), A. Kabla (Cambridge University), E. Cinquemani, H. de Jong, D. Ropers, J. Schaul, and S. Stoma (Institut National de Recherche en Informatique et en Automatique). We acknowledge the support of the Agence Nationale de la Recherche (under the references DiSiP-ANR-07-JCJC-0001 and ICEBERG-ANR-10-BINF-06-01), of the Région Ile de France (C'Nano-ModEnv), of the Action d'Envergure ColAge from INRIA/INSERM (Institut Nationale de la Santé et de la Recherche Médicale), of the MechanoBiology Institute, and of the Laboratoire International Associé CAFS (Cell Adhesion France-Singapour).

1. Bhalla US, Ram PT, Iyengar R (2002) MAP kinase phosphatase as a locus of flexibility in a mitogen-activated protein kinase signaling network. *Science* 297:1018–1023.
2. Hooshangi S, Thiberge S, Weiss R (2005) Ultrasensitivity and noise propagation in a synthetic transcriptional cascade. *Proc Natl Acad Sci USA* 102:3581–3586.
3. Cai L, Dalal CK, Elowitz MB (2008) Frequency-modulated nuclear localization bursts coordinate gene regulation. *Nature* 455:485–490.
4. Celani A, Vergassola M (2010) Bacterial strategies for chemotaxis response. *Proc Natl Acad Sci USA* 107:1391–1396.
5. Baumgartner BL, et al. (2011) Antagonistic gene transcripts regulate adaptation to new growth environments. *Proc Natl Acad Sci USA* 108:21087–21092.
6. O'Shaughnessy EC, Palani S, Collins JJ, Sarkar CA (2011) Tunable signal processing in synthetic MAP kinase cascades. *Cell* 144:119–131.
7. Walter E, Pronzato L (1997) *Identification of Parametric Models from Experimental Data* (Springer, Berlin).
8. Bennett MR, et al. (2008) Metabolic gene regulation in a dynamically changing environment. *Nature* 454:1119–1122.
9. Hersen P, McClean MN, Mahadevan L, Ramanathan S (2008) Signal processing by the HOG MAP kinase pathway. *Proc Natl Acad Sci USA* 105:7165–7170.
10. Muzzey D, Gómez-Uribe CA, Mettetal JT, van Oudenaarden A (2009) A systems-level analysis of perfect adaptation in yeast osmoregulation. *Cell* 138:160–171.
11. Shimizu TS, Tu Y, Berg HC (2010) A modular gradient-sensing network for chemotaxis in Escherichia coli revealed by responses to time-varying stimuli. *Mol Syst Biol* 6:382.
12. Pelet S, et al. (2011) Transient activation of the HOG MAPK pathway regulates bimodal gene expression. *Science* 332:732–735.
13. Rao CV (2012) Expanding the synthetic biology toolbox: Engineering orthogonal regulators of gene expression. *Curr Opin Biotechnol*, 10.1016/j.copbio.2011.12.015.
14. Voigt CA (2006) Genetic parts to program bacteria. *Curr Opin Biotechnol* 17:548–557.
15. Khalil AS, Collins JJ (2010) Synthetic biology: Applications come of age. *Nat Rev Genet* 11:367–379.
16. Elowitz MB, Levine AJ, Siggia ED, Swain PS (2002) Stochastic gene expression in a single cell. *Science* 297:1183–1186.
17. Balázsi G, van Oudenaarden A, Collins JJ (2011) Cellular decision making and biological noise: From microbes to mammals. *Cell* 144:910–925.
18. Munsky B, Neuert G, van Oudenaarden A (2012) Using gene expression noise to understand gene regulation. *Science* 336:183–187.
19. Milias-Argeitis A, et al. (2011) In silico feedback for in vivo regulation of a gene expression circuit. *Nat Biotechnol* 29:1114–1116.
20. de Nadal E, Alepuz PM, Posas F (2002) Dealing with osmostress through MAP kinase activation. *EMBO Rep* 3:735–740.
21. Hohmann S (2002) Osmotic stress signaling and osmoadaptation in yeasts. *Microbiol Mol Biol Rev* 66:300–372.
22. Miermont A, Uhlendorf J, McClean M, Hersen P (2011) The dynamical systems properties of the HOG signaling cascade. *J Signal Transduct* 2011:930940.
23. Yi TM, Huang Y, Simon MI, Doyle J (2000) Robust perfect adaptation in bacterial chemotaxis through integral feedback control. *Proc Natl Acad Sci USA* 97:4649–4653.
24. Ferreira C, et al. (2005) A member of the sugar transporter family, Stl1p is the glycerol/H+ symporter in Saccharomyces cerevisiae. *Mol Biol Cell* 16:2068–2076.
25. O'Rourke SM, Herskowitz I (2004) Unique and redundant roles for HOG MAPK pathway components as revealed by whole-genome expression analysis. *Mol Biol Cell* 15:532–542.
26. Klipp E, Nordlander B, Krüger R, Gennemark P, Hohmann S (2005) Integrative model of the response of yeast to osmotic shock. *Nat Biotechnol* 23:975–982.
27. Hao N, et al. (2007) A systems-biology analysis of feedback inhibition in the Sho1 osmotic-stress-response pathway. *Curr Biol* 17:659–667.
28. Mettetal JT, Muzzey D, Gómez-Uribe C, van Oudenaarden A (2008) The frequency dependence of osmo-adaptation in Saccharomyces cerevisiae. *Science* 319:482–484.
29. Zi Z, Liebermeister W, Klipp E (2010) A quantitative study of the Hog1 MAPK response to fluctuating osmotic stress in Saccharomyces cerevisiae. *PLoS ONE* 5:e9522.
30. Zechner C, et al. (2012) Moment-based inference predicts bimodality in transient gene expression. *Proc Natl Acad Sci USA* 109:8340–8345.
31. Findeisen R, Imsland L, Allgower F, Foss BA (2003) State and output feedback nonlinear model predictive control: An overview. *Eur J Control* 9:179–195.
32. Tamás MJ, et al. (1999) Fps1p controls the accumulation and release of the compatible solute glycerol in yeast osmoregulation. *Mol Microbiol* 31:1087–1104.
33. Csete ME, Doyle JC (2002) Reverse engineering of biological complexity. *Science* 295:1664–1669.
34. Iglesias PA, Ingalls BP (2009) *Control Theory and Systems Biology* (MIT Press, Cambridge, MA).
35. Uhlendorf J, Bottani S, Fages F, Hersen P, Batt G (2011) Towards real-time control of gene expression: Controlling the hog signaling cascade. *Pac Symp Biocomput* 2011:338–349.
36. Menolascina F, di Bernardo M, di Bernardo D (2011) Analysis, design and implementation of a novel scheme for in-vivo control of synthetic gene regulatory network. *Automatica* 47:1265–1270.
37. Toettcher JE, Gong D, Lim WA, Weiner OD (2011) Light-based feedback for controlling intracellular signaling dynamics. *Nat Methods* 8:837–839.
38. Regot S, et al. (2011) Distributed biological computation with multicellular engineered networks. *Nature* 469:207–211.
39. Sprinzak D, et al. (2010) Cis-interactions between Notch and Delta generate mutually exclusive signalling states. *Nature* 465:86–90.
40. Edelstein A, Amodaj N, Hoover K, Vale R, Stuurman N (2010) Computer control of microscopes using μManager. *Curr Protoc Mol Biol*, 10.1002/0471142727.mb1420s92.
41. Rasband WS (1997–2012) *ImageJ* (US National Institutes of Health, Bethesda, MD). Available at http://imagej.nih.gov/ij/. Accessed July 29, 2012.
42. Ballard DH (1981) Generalizing the Hough transform to detect arbitrary shapes. *Pattern Recognit* 13(2):111–122.